CrossMark

Decay modes of highly excited nuclei

Zhen-Fang Zhang[1,2] · De-Qing Fang[1] · Yu-Gang Ma[1]

Abstract The deexcitation of single excited ^{112}Sn nuclei at $T = 1$–30 MeV is simulated using the isospin-dependent quantum molecular dynamics (IQMD) model and GEMINI model. The fragmentation mechanism, critical behavior, and kinematic characteristics are investigated within these two models. The results show that the IQMD model can be applied to the analysis of fragmentation processes, critical points, and slope temperature extraction. The results of IQMD are generally consistent with experimental $\langle M_{\mathrm{IMF}} \rangle - Z_{\mathrm{bound}}$ data. However, GEMINI can reproduce the experimental data better than IQMD for isotopic distributions.

Keywords Excited nuclei · IQMD model · GEMINI model · Deexcitation

✉ De-Qing Fang
  dqfang@sinap.ac.cn

  Yu-Gang Ma
  ygma@sinap.ac.cn

[1] Shanghai Institute of Applied Physics, Chinese Academy of Sciences, Shanghai 201800, China

[2] University of Chinese Academy of Sciences, Beijing 100049, China

1 Introduction

Nuclear fragmentation in heavy-ion collisions is one of the most challenging subjects. Initially, the proton-induced reactions were found to produce fragments of all mass numbers [1]. Subsequently, the multifragmentation phenomenon was discovered. This phenomenon can be described as many particles heavier than α being produced at the same time in a single collision at energies above 30 MeV/nucleon [2]. Since then, many experiments and theoretical works have been dedicated for exploring the reaction mechanism. However, the phenomenon is still not fully understood [3–11].

In intermediate-energy heavy-ion collision processes, at first, the nuclear system is compressed and heated. Then, the system breaks up into several fragments, including light particles, during the expansion stage. Many theoretical models have been proposed to describe this reaction scenario. A brief introduction to these models can be found in Ref. [12]. One may treat it as a statistical process, which means that before the system disintegrates into lightly charged particles, neutrons, and intermediate mass fragments (IMFs) simultaneously, statistical equilibrium is reached in some subsystems during the expansion. This kind of equilibrium can be maintained until each subsystem becomes deexcited and the whole system reaches the freeze-out stage [3]. The final products are the sum of the decay results from all the subsystems.

To further understand this physical process, the isospin-dependent quantum molecular dynamics model (IQMD) [13, 14] and the GEMINI statistical model [15] are adopted to investigate the decay process. The combination of IQMD and GEMINI is applied in many articles to obtain isotopic distributions which are close to

experimental data. In this combination, the expansion dynamics are done by IQMD and GEMINI is just used for the decay of the fragments produced by IQMD. Hubele et al. [16] also emphasized that it is necessary to have a complete dynamical treatment of the decay process. To compare the decay processes between the two models, it is interesting to study the deexcitation of a single excited nucleus within IQMD and GEMINI. In this way, the influences of the parameters and approximations employed in these models could be reduced [17]. By comparing them with the experimental data, it can be learned how well the IQMD and GEMINI models can describe the deexcitation processes of excited nuclei.

This paper is organized as follows: a brief introduction to the IQMD and GEMINI models is given in Sect. 2. In Sect. 3, the calculated results and discussions are presented. Finally, the conclusions are given in Sect. 4.

2 Model description

2.1 Dynamical model: IQMD

The QMD model is a many-body theory that describes two-nuclei collisions from intermediate to relativistic energies. The IQMD model, which is based on QMD, has been successfully applied to heavy-ion collisions with consideration of the isospin degree-of-freedom for nucleons [18, 19]. The nucleons are represented by Gaussian wave packets with width L ($L = 2.16$ fm^2). When the nucleons propagate in the mean field, they are governed by the following potential:

$$
\begin{aligned}
U(\rho, \tau_z) = {} & \alpha\left(\frac{\rho}{\rho_0}\right) + \beta\left(\frac{\rho}{\rho_0}\right)^{\gamma} + \frac{1}{2}(1 - \tau_z)V_c \\
& + C_{\text{sym}}\frac{(\rho_n - \rho_p)}{\rho_0}\tau_z + U^{\text{Yuk}} + U^{\text{MDI}},
\end{aligned}
\tag{1}
$$

where $\alpha = -390.1$ MeV, $\beta = 320.3$ MeV, and $\gamma = 1.14$ are the momentum-dependent nuclear equation of state (EOS) parameters, with an incompressibility of $K = 200$ MeV [14]. ρ, ρ_0, ρ_n, and ρ_p are the total, normal, neutron, and proton densities, respectively. τ_z (=1 for neutron or -1 for proton) is the zth component of the isospin degree-of-freedom. V_c is the Coulomb potential and C_{sym} is the strength of the symmetry energy, which equals 32 MeV. The last two parameters, U^{Yuk} and U^{MDI}, represent the Yukawa potential and the momentum-dependent interaction, respectively.

In this work, a single excited nuclear source is simulated at different temperatures. Usually, the initial nucleus is in the state $T = 0$ (T is the temperature), corresponding to the ground state. The moment distribution is calculated with the Fermi gas approximation $P_{\text{F}}^i(\vec{r}) = \hbar[3\pi^2\rho_i(\vec{r})]^{1/3}$ after its initial coordinate is sampled by the Monte Carlo method. ρ_i ($i = n$ or p) is the local density of neutrons or protons, respectively. To study the states of nuclei with $T > 0$, we replace the previous moment distribution with the Fermi–Dirac distribution,

$$
n(e_k) = \frac{g(e_k)}{e^{\frac{e_k - \mu}{T}} + 1},
\tag{2}
$$

where $e_k = \frac{p^2}{2m}$ is the state kinetic energy. p and m represent the momentum and mass of the nucleon, respectively. $g(e_k) = \frac{V}{2\pi^2}\left(\frac{2m}{\hbar^2}\right)^{\frac{3}{2}}\sqrt{e_k}$ is the state density. $V = \frac{4}{3}\pi r^3$, with $r = r_0 A^{1/3}$, is the volume of the source, and the source radius r is determined by the radius parameter r_0 and nuclear mass A. μ is the chemical potential, which is determined by the following integral equation:

$$
\frac{1}{2\pi^2}\left(\frac{2m}{\hbar^2}\right)^{\frac{3}{2}}\int_0^{\infty}\frac{\sqrt{e_k}}{e^{\frac{e_k - \mu_i}{T}} + 1}\,\mathrm{d}e_k = \rho_i.
\tag{3}
$$

In this paper, the simulated temperatures are from 1 to 30 MeV and the excited nucleus evolves in the mean field without collisions after the initialization [20].

2.2 Statistical model: GEMINI

GEMINI is a Monte Carlo code written in 1986 that follows the decay of a compound nucleus through a series of sequential binary decays like light-particle evaporation and symmetric fission. All possible binary decays are performed until the resulting products cannot decay any further [15]. There are four basic parameters as the input: fragment mass number A, charge number Z, excitation energy E^*, and angular moment L. To study the same excited nuclear source, the excitation energy and angular moment of the hot nucleus are calculated in the IQMD when the initialization is just completed:

$$
\vec{L}_i = \vec{R}_i \times \vec{P}_i,
\tag{4}
$$

$$
E^* = E_{\text{bind}}^{\text{excited}} - E_{\text{bind}}^{\text{ground}}.
\tag{5}
$$

$\vec{R}_i$ and $\vec{P}_i$ are vectors of the coordinates and momentum, respectively, and i represents the ith nucleon of the nucleus [21]. $E_{\text{bind}}^{\text{excited}}$ is the binding energy of the excited nucleus and it can be calculated from the IQMD model. The $E_{\text{bind}}^{\text{ground}}$ is obtained from the nuclear data table [22]. The latest atomic mass evaluation can be seen in Ref. [23].

3 Results and discussion

In this section, the fragmentation mechanisms are first analyzed. Then, the critical behavior and slope temperature are compared between the two models. Finally, the comparison of the results between the calculated and experimental data are discussed. In this work, a nuclear source of normal density with 50 protons and 62 neutrons (^{112}Sn) is chosen. The simulation in IQMD is calculated up to 200 fm/c and the number of simulated events is 1000 for each temperature point. The fragments are constructed by a coalescence model, in which nucleons with relative distances smaller than 3.5 fm and relative momenta smaller than 300 MeV/c are combined into one cluster [24].

3.1 Fragmentation mechanism

Before comparing the fragmentation phenomena of the two models, it has to be checked whether the time-length of 200 fm/c is sufficient for the nucleus decay in IQMD. This question is investigated by looking at the mean multiplicity and production rate of the IMFs, which is defined as the fragments with $3 \leq Z \leq 20$.
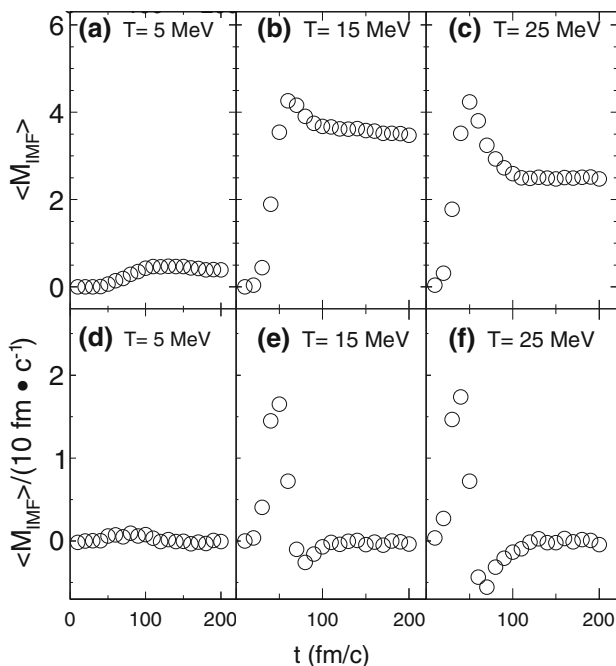

Fig. 1 Mean multiplicity of the IMFs (upper panels) and the production rate of the mean multiplicity of the IMFs (bottom panels) at 5, 15, and 25 MeV, respectively. The evolution time is up to 200 fm/c. As the fragment data are output every 10 fm/c in our calculation, the production rate is defined as the variation in the mean multiplicity of the IMFs every 10 fm/c. The production rate at t_i is calculated by $\mathrm{IMF}_{t_i} - \mathrm{IMF}_{t_{i-1}}$ ($i = 1, 2, 3, \ldots, 20$). IMF_{t_i} is the mean multiplicity of the IMFs at t_i ($t_i = 0$ fm/c, 10 fm/c, 20 fm/c, $\ldots$, 200 fm/c)

From Fig. 1, it is found that the $\langle M_{\mathrm{IMF}} \rangle$ remains almost the same after 100 fm/c at different temperatures. The production rates of the IMFs become almost zero after 100 fm/c. It indicates that the fragment formation is finished within 100 fm/c and the evolution time of 200 fm/c is enough in IQMD.

Figure 2 presents the mean multiplicity of the IMFs calculated by IQMD and GEMINI at different temperatures. They have very similar trends at lower temperatures, but the maximum value of the mean IMF multiplicity of IQMD is much bigger than that of GEMINI. The T-value corresponding to the maximum value of the mean IMF multiplicity is also higher for IQMD. In addition, nuclei in IQMD can keep the fragments' structure, while they are almost completely disassembled into light particles in GEMINI at very high temperatures. The inset graph shows the correlation between the temperature and mean excitation energy calculated by Eq. (5). It is similar to a Fermi gas curve at low excitation energies and shows linear growth at high excitation energies. Thus, the excitation energies of the nuclei used as input for GEMINI at different temperatures are reasonable in this respect.

To conveniently compare the fragmentation mechanisms between the two models at different temperatures, three fragmentation phenomena, i.e., spallation, fission, and multifragmentation, are distinguished by the multiplicity M_{H} of the heavy fragments in a single event: $M_{\mathrm{H}} = 1$ for spallation, $M_{\mathrm{H}} = 2$ for fission, and $M_{\mathrm{H}} = 0$ with at least one fragment of $Z > 2$ for multifragmentation. Fragments with $Z > 20$ are defined as heavy fragments [25]. It is well known that the binary decay modes that cause the particles evaporated one-by-one from the
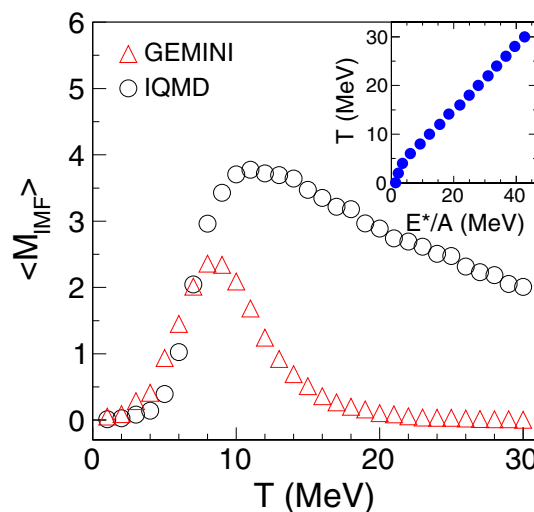

Fig. 2 Temperature dependence of the mean multiplicity of the IMFs for IQMD (circles) and GEMINI (triangles). The correlation between the excitation energy per nucleon and temperature is shown in the inset graph

excited nuclei are adopted in the GEMINI code. Thus, the multifragmentation that is caused by chemical instability cannot be treated with GEMINI. Here, the multifragmentation only concerns the decay results for GEMINI.

In Fig. 3, the fractions of spallation, fission, and multifragmentation at different temperatures are presented for IQMD and GEMINI. Fission is a rare process that only occurs at lower temperatures. It is interesting to see the opposing trends of the spallation and multifragmentation below $T = 10$ MeV. There exists an apparent deviation between IQMD and GEMINI in the multifragmentation. The deviation corresponds to the discrepancy in the mean multiplicity of the IMFs at high temperatures, as we can see in Fig. 2. In general, the main fragmentation phenomena are similar in IQMD and GEMINI, which indicates that a statistical model and dynamical model may obtain comparable results for the decay process.
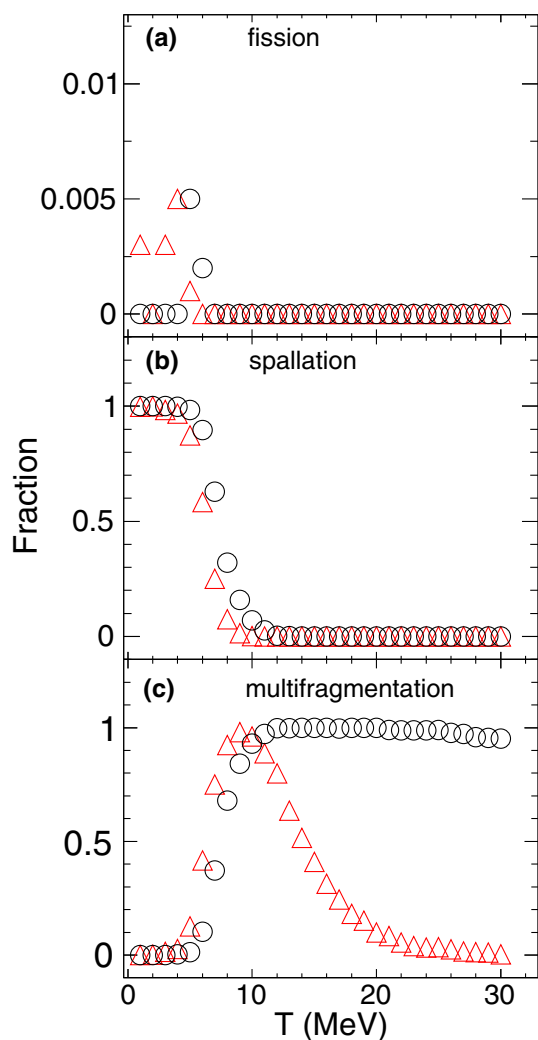
3.2 Critical behavior

It is a significant topic in nuclear physics to explore the liquid–gas phase transition of finite nuclei that is associated with the nuclear equation of state and clarification of the mechanism when a heated nucleus disassembles [26, 27]. Many signatures have been applied to identify the critical region. The Fisher droplet model is extensively used in the study of multifragmentation, and the extracted value of the power-law exponent is reasonable for the critical behavior analysis [28, 29]. We employed a power-law fit for the charge distribution in the range $Z = 2$–7 for IQMD and $Z = 1$–7 for GEMINI. The effective Fisher-law parameter τ_{eff} is extracted from the following equation:

$$\mathrm{d}N/\mathrm{d}Z \sim Z^{-\tau_{\text{eff}}}. \tag{6}$$

The upper and bottom panels of Fig. 4 show the charge distributions at $T = 5$, 15, and 25 MeV for GEMINI and IQMD, respectively. The charge distributions become steeper with increasing temperatures, and the widths of the charge distributions of GEMINI are narrower than those of IQMD. The fitting curves are consistent with the IQMD data, but the fitting curves for GEMINI are not very good, and the errors of τ_{eff} are quite large, as presented in Fig. 5. Thus, the charge distributions of GEMINI are not well described by the power-law dependence.

The overall trend for τ_{eff} with temperature is that it first falls to a minimum at about 8 MeV for GEMINI and 10 MeV for IQMD and then rises slowly. The minimum values of τ_{eff} are 1.79 for GEMINI and 2.14 for IQMD,

Fig. 3 Fractions of fragmentation phenomena (fission, spallation, and multifragmentation) at different temperatures. The triangles represent the results of GEMINI, and the circles correspond to IQMD results
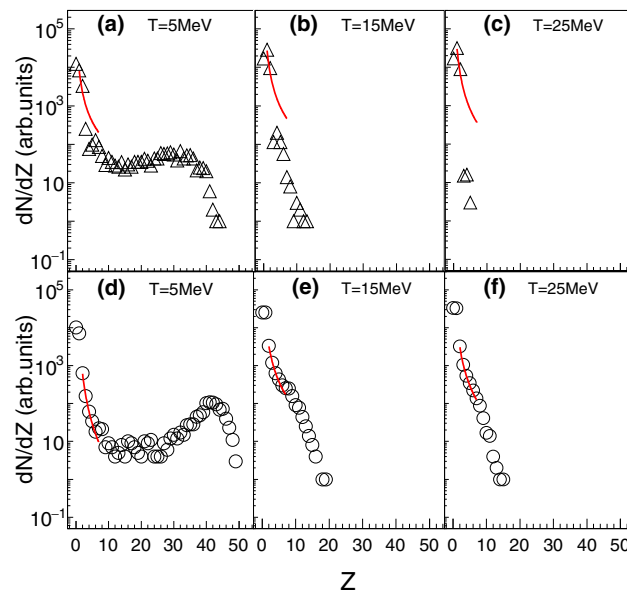

Fig. 4 Charge distributions at $T = 5$, 15, and 25 MeV. The results of GEMINI are given in the upper panels. The same distributions by IQMD are shown in the bottom panels. The lines are the power-law fits for $2 \leq Z \leq 7$ (IQMD) and $1 \leq Z \leq 7$ (GEMINI)
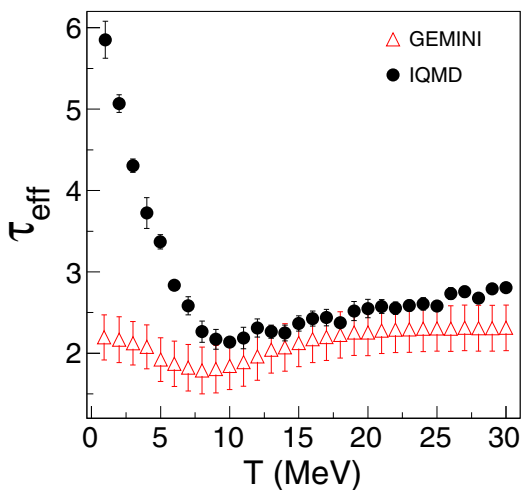
Fig. 5 Extracted τ_{eff} parameters at different temperatures for GEMINI (triangles) and IQMD (dots)

Fig. 6 Campi plots at different temperatures for GEMINI (upper panels) and IQMD (bottom panels)

respectively. The Fisher droplet model predicted a reasonable critical exponent ~ 2.21 for the critical behavior [28]. The result of IQMD is closer to the critical exponent. It indicates that the critical behavior is better presented within IQMD model and a possible critical point around $T = 10$ MeV.

The occurrence of the largest fluctuation indicates that the system undergoes a continuous transition. Campi has suggested using the event-by-event distribution of the logarithm of the largest fragment's size versus the normalized second moment. The normalized second moment is represented by S_2 with the heaviest fragment removed,

$$S_2 = \frac{\sum_{Z_i \neq Z_{max}} Z_i^2 \cdot n_i(Z_i)}{\sum_{Z_i \neq Z_{max}} Z_i \cdot n_i(Z_i)}. \tag{7}$$

Z_i is the charge number of the ith fragment and $n_i(Z_i)$ is the multiplicity of fragment Z_i. Campi plots are presented in Fig. 6, and they are instructive for analyzing the critical behavior [30].

There are three selected temperatures for each model. At low temperatures, the upper branch, which represents the liquid phase, is strongly dominant. At $T = 15$ MeV, the lower Z_{max}, which represents the gas phase, is strongly dominant. The transition from the liquid-dominated branch to the vapor branch then occurs, which indicates that the region of maximal fluctuations is in the range of 5–15 MeV.

To further identify the critical point, we also introduce the quantity γ_2, which was suggested by Campi:

$$\gamma_2 = \frac{M_2 M_0}{M_1^2}, \tag{8}$$

$$M_k = \sum_{Z_i \neq Z_{max}} Z_i^k \cdot n_i(Z_i). \tag{9}$$

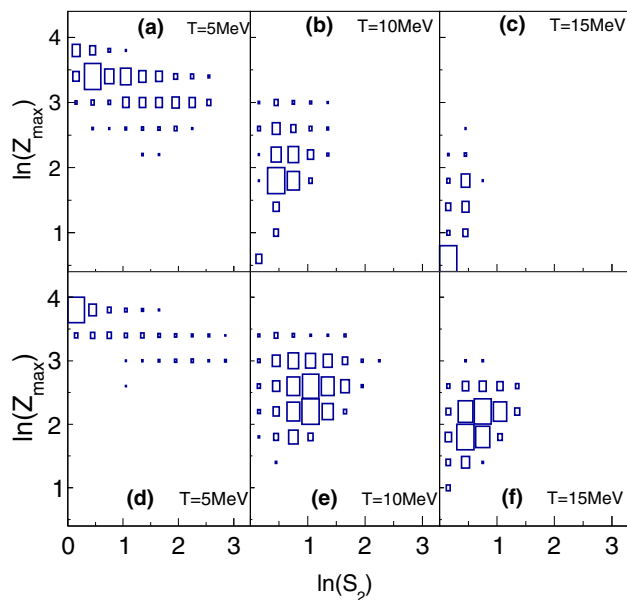M_0, M_1, M_2 and M_k are the zeroth, first, second, and kth moments of the charge distribution, respectively [31].

Figure 7 presents the temperature dependence of the average values of γ_2 obtained from the event-by-event analysis. There are well-defined peaks in γ_2 for both models, while the maximum value of γ_2 is larger for IQMD. The maximum values are reached at $T = 6$ and 8 MeV for GEMINI and IQMD, respectively. They are defined as the critical points where the largest fluctuations in fragment sizes are obtained. However, the peak value of γ_2 is expected to reach at least 2 for the critical behavior. Although a maximum value of γ_2 lower than 2 has been
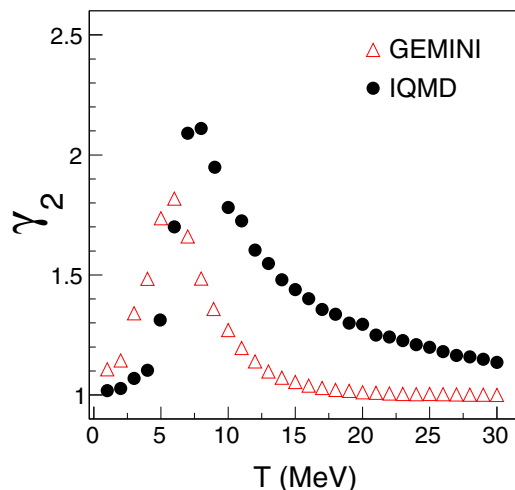

Fig. 7 Calculated values of γ_2 at different temperatures for GEMINI (the triangles) and IQMD (the dots)

observed in a light system with $A = 36$ [27], the value extracted by GEMINI in this work is suspect for such heavy system like ^{112}Sn. Thus, the most probable critical region is $T = 8$–10 MeV in our calculation.

3.3 Kinematic characteristic

Nuclear temperature is a concept derived from the compound nucleus definition [32]. The Coulomb [33, 34], recoil [35], and collective effects [36, 37] have been observed with the slope thermometer, whose value for the temperature is extracted from the distribution of the kinetic energy spectra. Figure 8 presents the kinetic energy spectra of ^{2}H at four temperatures for the two models, and the fitting curves are calculated by the surface-emission-type method [33]:

$$Y(E) \propto \frac{(E - E_0)}{T_{\text{slope}}^2} \exp\left[-\frac{(E - E_0)}{T_{\text{slope}}}\right], \quad (10)$$

where E_0 reflects the Coulomb repulsion.

As the temperature or excitation energy increases, the final kinetic energy distribution of ^{2}H becomes broader, but the peak positions of the spectra that are close to the Coulomb barriers seem to be insensitive to the temperature. This phenomenon can be explained by the fact that the
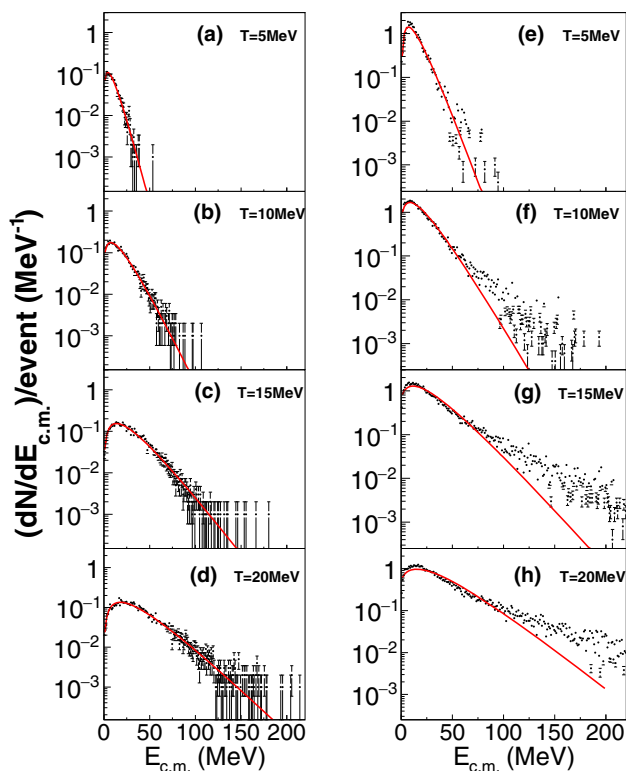
Coulomb barrier is dependent on the charge of the initial emitting source, which is fixed in the simulation [38, 39].

To further investigate the kinetic characteristics, the slope values of the center-of-mass kinetic energy spectra for H and He were extracted, which are shown in Fig. 9. One can observe that the slope temperatures are mass dependent for the IQMD model [6, 40, 41]. The extracted T_{slope} values increase with increasing mass numbers for the same elements that are associated with the radial flow effect. Usually, the Coulomb effect can be observed by comparing the T_{slope} values extracted from two fragments with the same mass number but different charge numbers. However, there is no obvious discrepancy between ^{3}H and ^{3}He. It may be that the Coulomb effect is not so apparent
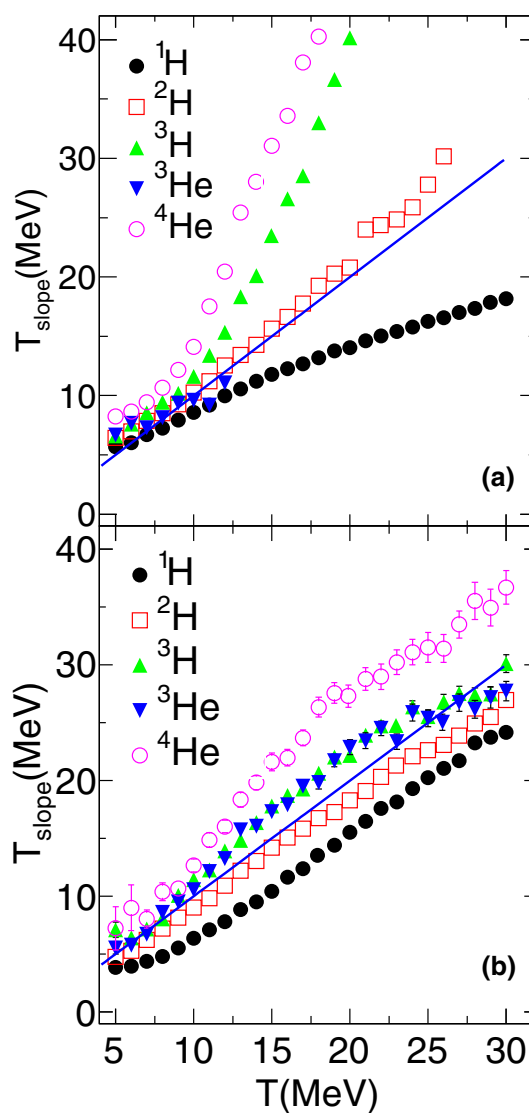
Fig. 8 Kinetic energy distributions of ^2H at $T = 5$, 10 , 15, and 20 MeV. The left panels are the IQMD results and the right ones are the GEMINI results

Fig. 9 Extracted slope temperatures for isotopes ^{1}H, ^{2}H, ^{3}H, ^{3}He, and ^{4}He, respectively. The upper and bottom panels correspond to the results of GEMINI and IQMD, respectively. The solid lines represent the initial given temperatures

for there is no compression process as in the collision reaction. The T_{slope} values of the neutron are also extracted, which are almost the same as those of the proton. Generally, the T_{slope} values of ^{4}He are lower than ^{3}He in the collision experiments for the abundant secondary emission of ^{4}He from heavy fragments. The ^{4}He production in different evolution times was checked, and there were no obvious decreases in the momentum distributions, which indicates that this effect is limited in the simulation. The results of GEMINI show similar mass dependent trends, but deviations between the fitting curves and calculated data occur with increasing temperatures, which can be seen in Fig. 8. The kinetic energy distributions of ^{3}He become rather dispersive at high temperatures, thus only several extracted values are given. In fact, the decay nucleus no longer acts like a thermal source for the increasing intensity of the sequential binary decay characteristic. Thus, the extracted T_{slope} values are more reliable in the lower temperature region for GEMINI. It is interesting to see that the T_{slope} values of ^{2}H are closest to the given temperatures for both models.

3.4 Comparison with experimental data

The projectile fragmentation of ^{124}Sn-on-^{nat}Sn at 600 MeV/nucleon has been studied with the ALADIN forward spectrometer at the GSI Schwerionen Synchrotron [42]. To quantitatively compare it with the experimental $\langle M_{IMF} \rangle$ versus Z_{bound} projectile data, where Z_{bound} is defined as the sum of the charges of all fragments with $Z \geq 2$ in a single event, a series of primary nuclear sources are mixed in the following way to simulate the excited residual nuclei produced in the experiment. First, the average mass of the equilibrated source $\overline{A}$ has the correlation with the excitation energy per nucleon E_x/A suggested by Botvina et al. [43]:

$$\alpha \equiv \frac{\overline{A}}{A_0} = 1 - 0.001(E_x/A) - 0.015(E_x/A)^2, \quad (11)$$

where A is assumed to have a Gaussian distribution around $\overline{A}$ and A_0 is the mass number of the projectile. The width of the distribution is decided by the following formula:

$$\sigma = \sigma_0 A_0 \left(1 + c_0 \frac{\epsilon^2}{\epsilon_{max}^2}\right) \quad (12)$$

$\epsilon = E_x/A$ and ϵ_{max} represents the maximum value of ϵ. The parameters ϵ_{max}, σ_0, and c_0 are 8.13 MeV, 0.07, and 2, respectively, in the simulation and the details can be seen in Refs. [42, 43]. Then, the distribution of the mass versus excitation energy is generated with the two equations above, as shown in Fig. 10.

Next, 20 primary nuclear sources are chosen with initial temperatures derived from the correlation of the excitation

energy and temperature. As the correlation is not precise, integer temperature values are adopted. The specific mass numbers and mixed proportions of the nuclear sources are presented in Fig. 11. The charge numbers of the different sources are obtained with the N/Z ratio remaining the same as the projectile ^{124}Sn. The parameters of the nuclear sources are identical for the two models.

In Fig. 12, it can be seen that the simulated results of IQMD are generally consistent with the experimental data, while the results of GEMINI show apparent deviations. However, the rising and falling trends of the GEMINI data are close to the experimental data. Thus, it is reasonable continue exploring the isotopic distribution.

As there is no impact parameter in the single nucleus decay process, the yields of the isotopes cannot be compared with the experimental cross sections. However, the peak position and shape of the distribution are important information. Thus, the relative yield is studied, where the isotope with the highest yield is set to 1.

In Fig. 13, the shapes of the isotopic distributions by GEMINI are very close to the experimental data, while those of IQMD are much wider. To quantitatively compare the parameters of the isotopic distributions between the two models, the average mass numbers and the standard deviations σ of the mass numbers for all isotopes in the events with $10 \leq Z_{bound} \leq 40$ are presented in Fig. 14.

The average mass numbers of the isotopes for different charge numbers Z are almost the same for IQMD and GEMINI. The σ is much larger for IQMD, which means a broader isotopic distribution. It may be that the final fragments in the IQMD model do not completely reach the ground state while the experimental fragments are in the
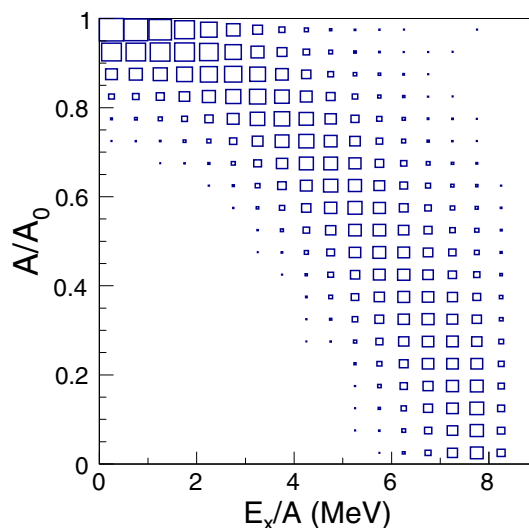

Fig. 10 Mass number versus excitation energy distribution of different thermal sources calculated with Eqs. (11) and (12). The numbers of the sources are proportional to the areas of the squares
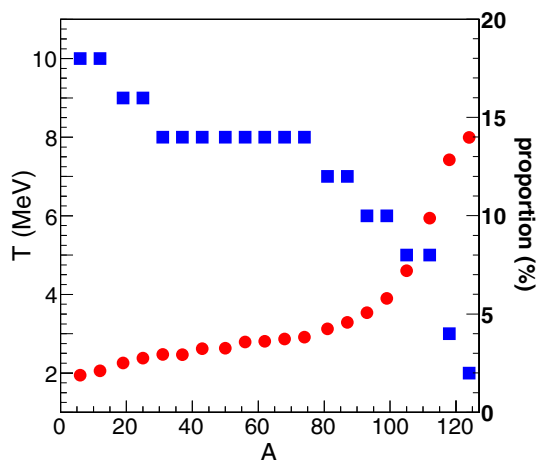
Fig. 11 Proportions and temperatures of different nuclear sources adopted to simulate the excited residual nuclei produced in a 600 MeV/nucleon ^{124}Sn-on-^{nat}Sn experiment. A is the mass number of the different nuclear sources. The solid squares represent the temperatures of the nuclear sources. The proportions of the different sources used for the simulation are presented with dots
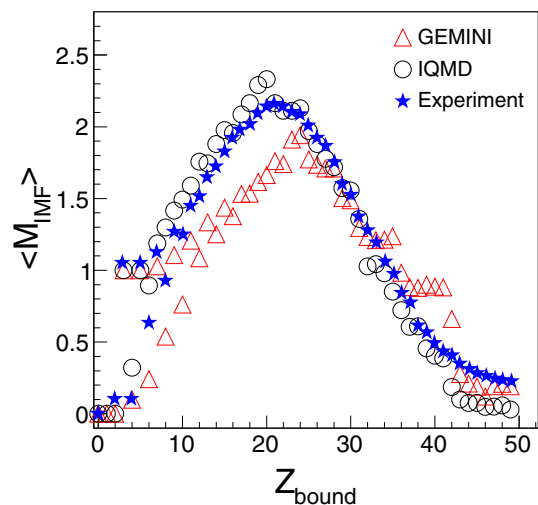

Fig. 12 Distributions of $\langle M_{IMF}\rangle$ versus Z_{bound} by IQMD and GEMINI compared with the experimental results in Ref. [42]. The stars represent experimental data. The circles and triangles are the calculated results with a series of mixed nuclear sources by IQMD and GEMINI, respectively

ground state. In the GEMINI model, extensive comparisons with data from a large range of compound-nucleus masses have been used to optimize the default parameters. The good overall agreement with the experimental data for the isotopic distributions in the calculations by GEMINI can be attributed to this.
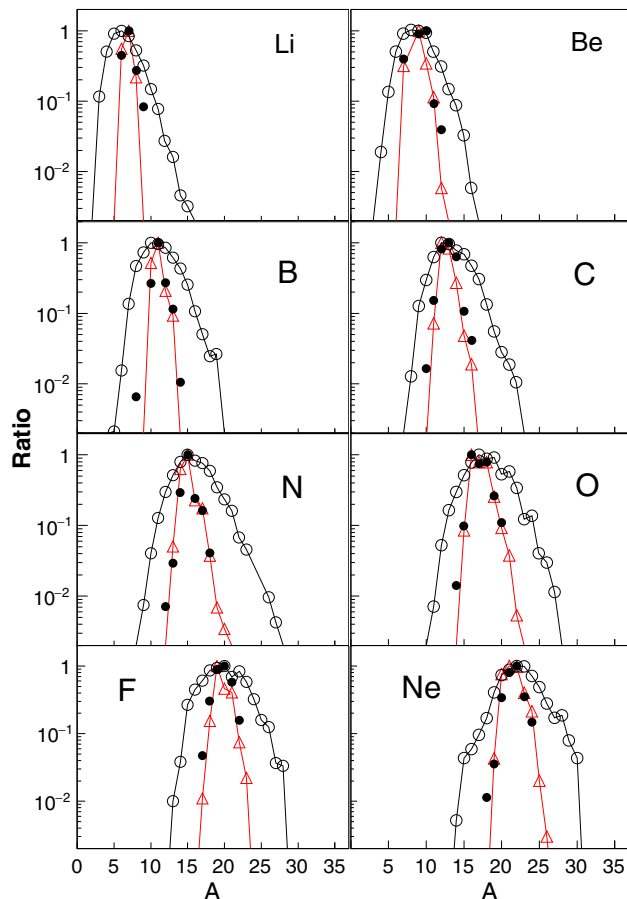

Fig. 13 Isotopic distributions of $Z = 3$–10. The yields are replaced by defined ratios where the highest yield is set to 1. The dots are experimental data integrated over $10 \leq Z_{bound} \leq 40$. The circles and triangles are the calculated results of IQMD and GEMINI, respectively. The lines are for clarity

4 Conclusion

The deexcitation processes of single excited ^{112}Sn nuclei are simulated at $T = 1$–30 MeV with a dynamical model (IQMD) and a statistical model (GEMINI). The fragmentation mechanisms, critical behavior, and kinematic characteristics are investigated, and some results are compared with experimental data. It is found that IQMD and GEMINI give similar fragmentation phenomena in different temperature regions. However, the power-law fit and the extraction of γ_2 are more reasonable with the IQMD model. Moreover, the extracted slope temperatures of IQMD are more reasonable and closer to the original temperatures than those of GEMINI, which indicates a better kinematic description. The simulation results of IQMD with mixed thermal sources are consistent with experimental $\langle M_{IMF}\rangle - Z_{bound}$ data of the projectiles, but GEMINI can reproduce the widths of the experimental isotopic distributions better than IQMD.
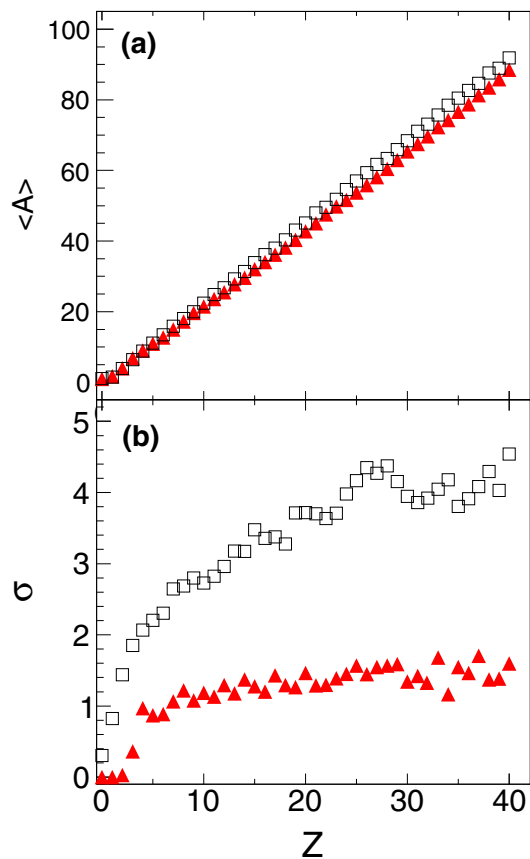
Fig. 14 Average mass numbers $\langle A \rangle$ of the isotopes with different charge numbers Z in the events with $10 \leq Z_{bound} \leq 40$ are plotted in the top panel and the corresponding standard deviations σ are presented in the bottom panel. The squares and solid triangles are the results of IQMD and GEMINI, respectively

In general, both IQMD and GEMINI could be used to explore the decay properties of excited nuclei like the fragment distributions or fragmentation mechanisms. However, the multifragmentation phenomenon, which is related to the chemical instability, cannot be treated with GEMINI. The critical phenomena and kinematic characteristics are also associated with dynamical behaviors. Thus, they might be better described within the IQMD model. However, GEMINI shows advantages in reproducing isotopic distributions.

Thus, the IQMD model can reproduce the decay properties of an excited nucleus rather well, and it is shown that the IQMD model can be used alone in most cases.

References

1. S.B. Kaufman, M.W. Weisfield, E.P. Steinberg et al., Nuclear reactions of ^{197}Au with 11.5- and 300-GeV protons. Phys. Rev. C **14**, 1121 (1976). https://doi.org/10.1103/PhysRevC.14.1121

2. A.I. Warwick, H.H. Wiemann, H.H. Gutbrod et al., Breakup of spectator residues in relativistic nuclear collisions. Phys. Rev. C **27**, 1083 (1983). https://doi.org/10.1103/PhysRevC.27.1083

3. R. Nebauer, J. Aichelin, Multifragmentation—what the data tell us about the different models. Nucl. Phys. A **681**, 353 (2001). https://doi.org/10.1016/S0375-9474(00)00539-X

4. D.Q. Fang, W.Q. Shen, J. Feng et al., Isospin effect of fragmentation reactions induced by intermediate energy heavy ion and its disappearance. Phys. Rev. C **61**, 044610 (2000). https://doi.org/10.1103/PhysRevC.61.044610

5. N. Marie, A. Chbihi, J.B. Natowitz et al., Experimental determination of fragment excitation energies in multifragmentation events. Phys. Rev. C **58**, 256 (1998). https://doi.org/10.1103/PhysRevC.58.256

6. T.T. Ding, C.W. Ma, An improved thermometer for intermediate-mass fragments. Nucl. Sci. Tech. **27**, 132 (2016). https://doi.org/10.1007/s41365-016-0142-2

7. K. Hagel, M. Gonin, R. Wada et al., Violent collisions and multifragment final states in the ^{40}Ca + ^{40}Ca reaction at 35 MeV/nucleon. Phys. Rev. C **50**, 2017 (1994). https://doi.org/10.1103/PhysRevC.50.2017

8. M. Mocko, M.B. Tsang, L. Andronenko et al., Projectile fragmentation of ^{40}Ca, ^{48}Ca, ^{58}Ni, and ^{64}Ni at 140 MeV/nucleon. Phys. Rev. C **74**, 054612 (2006). https://doi.org/10.1103/PhysRevC.74.054612

9. P. Liu, J.H. Chen, Y.G. Ma et al., Production of light nuclei and hypernuclei at high intensity accelerator facility energy region. Nucl. Sci. Tech. **28**, 55 (2017). https://doi.org/10.1007/s41365-017-0207-x

10. R. Ogul, N. Buyukcizmeci, A. Ergun et al., Production of neutron-rich exotic nuclei in projectile fragmentation at Fermi energies. Nucl. Sci. Tech. **28**, 18 (2016). https://doi.org/10.1007/s41365-016-0175-6

11. Z.Q. Feng, Nuclear dynamics and particle production near threshold energies in heavy-ion collisions. Nucl. Sci. Tech. **29**, 40 (2018). https://doi.org/10.1007/s41365-018-0379-z

12. C.W. Ma, Y.G. Ma, Shannon information entropy in heavy-ion collisions. Prog. Part. Nucl. Phys. **99**, 120 (2018). https://doi.org/10.1016/j.ppnp.2018.01.002

13. J. Aichelin, "Quantum" molecular dynamics—a dynamical microscopic n-body approach to investigate fragment formation and the nuclear equation of state in heavy ion collisions. Phys. Rep. **202**, 233 (1991). https://doi.org/10.1016/0370-1573(91)90094-3

14. C. Hartnack, R.K. Puri, J. Aichelin et al., Modelling the many-body dynamics of heavy ion collisions: present status and future perspective. Eur. Phys. J. A **1**, 151 (1998). https://doi.org/10.1007/s100500050045

15. R.J. Charity, M.A. McMahan, G.J. Wozniak et al., Systematics of complex fragment emission in niobium-induced reactions. Nucl. Phys. A **483**, 371 (1988). https://doi.org/10.1016/0375-9474(88)90542-8

16. J. Hubele, P. Kreutz, V. Lindenstruth et al., Statistical fragmentation of Au projectiles at E/A = 600 MeV. Phys. Rev. C **46**, 1577 (1992). https://doi.org/10.1103/PhysRevC.46.R1577

17. W. Müller, M. Begemann-Blaich, J. Aichelin, Deexcitation of single excited nuclei in the QMD model. Phys. Lett. B **298**, 27 (1993). https://doi.org/10.1016/0370-2693(93)91700-W

18. X.G. Cao, X.Z. Cai, Y.G. Ma et al., Nucleon–nucleon momentum–correlation function as a probe of the density distribution of valence neutrons in neutron–rich nuclei. Phys. Rev. C **86**, 044620 (2012). https://doi.org/10.1103/PhysRevC.86.044620

19. X.Y. Sun, D.Q. Fang, Y.G. Ma et al., Neutron/proton ratio of nucleon emissions as a probe of neutron skin. Phys. Lett. B **682**, 396 (2010). https://doi.org/10.1016/j.physletb.2009.11.031

20. D.Q. Fang, Y.G. Ma, C.L. Zhou, Shear viscosity of hot nuclear matter by the mean free path method. Phys. Rev. C **89**, 047601 (2014). https://doi.org/10.1103/PhysRevC.89.047601

21. Z.T. Dai, D.Q. Fang, Y.G. Ma et al., Effect of neutron skin thickness on projectile fragmentation. Phys. Rev. C **91**, 034618 (2015). https://doi.org/10.1103/PhysRevC.91.034618

22. G. Audi, A.H. Wapstra, C. Thibault, The Ame 2003 atomic mass evaluation: (II). Tables, graphs and references. Nucl. Phys. A **729**, 337 (2003). https://doi.org/10.1016/j.nuclphysa.2003.11.003

23. M. Wang, G. Audi, F.G. Kondev et al., The AME2016 atomic mass evaluation (II). Tables, graphs and references. Chin. Phys. C **41**, 030003 (2017). https://doi.org/10.1088/1674-1137/41/3/030003

24. T.Z. Yan, Y.G. Ma, X.Z. Cai et al., Scaling of anisotropic flows and nuclear equation of state in intermediate energy heavy ion collisions. Chin. Phys. **16**, 9 (2007). https://doi.org/10.1088/1009-1963/16/9/031

25. C. Lewenkopf, J. Dreute, A. Abul-Magd et al., Fragmentation of gold projectiles with energies of 200–980 MeV/nucleon. II. Multiplicity distributions and correlations. Phys. Rev. C **44**, 1065 (1991). https://doi.org/10.1103/PhysRevC.44.1065

26. J.B. Natowitz, R. Wada, K. Hagel et al., Caloric curves and critical behavior in nuclei. Phys. Rev. C **65**, 034618 (2002). https://doi.org/10.1103/PhysRevC.65.034618

27. Y.G. Ma, J.B. Natowitz, R. Wada et al., Critical behavior in light nuclear systems: experimental aspects. Phys. Rev. C **71**, 054606 (2005). https://doi.org/10.1103/PhysRevC.71.054606

28. M.E. Fisher, The theory of equilibrium critical phenomena. Rep. Prog. Phys. **30**, 615 (1969). https://doi.org/10.1088/0034-4885/31/1/508

29. J.E. Finn, S. Agarwal, A. Bujak et al., Nuclear fragment mass yields from high-energy proton–nucleus interactions. Phys. Rev. Lett. **49**, 1321 (1982). https://doi.org/10.1103/PhysRevLett.49.1321

30. X. Campi, Multifragmentation: nuclei break up like percolation clusters. J. Phys. A **19**, 917 (1986). https://doi.org/10.1088/0305-4470/19/15/010

31. X. Campi, H. Krivine, Observables in nuclear fragmentation. Z. Phys. A **344**, 81 (1992). https://doi.org/10.1007/BF01291024

32. N. Bohr, Neutron capture and nuclear constitution. Nature **137**, 351 (1936). https://doi.org/10.1038/137344a0

33. P.M. Milazzo, G. Vannini, M. Azzano et al., Temperature measurement of fragment emitting systems in Au + Au 35 MeV/nucleon collisions. Phys. Rev. C **58**, 953 (1998). https://doi.org/10.1103/PhysRevC.58.953

34. T. Odeh, R. Bassini, M. Begemann-Blaich et al., Fragment kinetic energies and modes of fragment formation. Phys. Pev. Lett. **84**, 4557 (2000). https://doi.org/10.1103/PhysRevLett.84.4557

35. A.S. Hirsh, A. Bujak, J.E. Finn et al., Experimental results from high energy proton–nucleus interactions, critical phenomena, and the thermal liquid drop model of fragment production. Phys. Rev. C **29**, 508 (1984). https://doi.org/10.1103/PhysRevC.29.508

36. P.J. Siemens, J.O. Rasmussen, Evidence for a blast wave from compressed nuclear matter. Phys. Rev. Lett. **42**, 880 (1979). https://doi.org/10.1103/PhysRevLett.42.880

37. K.S. Lee, U. Heinz, E. Schnedermann, Search for collective transverse flow using particle transverse momentum spectra in relativistic heavy-ion collisions. Z. Phys. C **48**, 525 (1990). https://doi.org/10.1007/BF01572035

38. J. Su, L. Zhu, W.J. Xie et al., Nuclear temperatures from kinetic characteristics. Phys. Rev. C **85**, 017604 (2012). https://doi.org/10.1103/PhysRevC.85.017604

39. C.C. Guo, J. Su, F.S. Zhang, Comparison between nuclear thermometers in central Xe + Sn collision. Nucl. Sci. Technol. **24**, 050513 (2013). https://doi.org/10.13538/j.1001-8042/nst.2013.05.013

40. X. Liu, W. Lin, M. Huang et al., Freezeout concept and dynamical transport model in intermediate-energy heavy-ion reactions. Phys. Rev. C **92**, 014623 (2015). https://doi.org/10.1103/PhysRevC.92.014623

41. X.Q. Liu, M.R. Huang, R. Wada et al., Symmetry energy extraction from primary fragments in intermediate heavy-ion collisions. Nucl. Sci. Tech. **26**, S20508 (2015). https://doi.org/10.13538/j.1001-8042/nst.26.S20508

42. R. Ogul, A.S. Botvina, U. Atav et al., Isospin-dependent multifragmentation of relativistic projectiles. Phys. Rev. C **83**, 024608 (2011). https://doi.org/10.1103/PhysRevC.83.024608

43. A.S. Botvina, I.N. Mishustin, M. Begemann-Blaich et al., Multifragmentation of spectators in relativistic heavy-ion reactions. Nucl. Phys. A **584**, 737 (1995). https://doi.org/10.1016/0375-9474(94)00621-S